Water Air Soil Pollut (2020) 231: 37
https://doi.org/10.1007/s11270-020-4411-7

Naproxen Removal Capacity Enhancement by Transforming the Activated Carbon into a Blended Composite Material

Somen Mondal · Surabhi Patel · Subrata Kumar Majumder

Received: 25 September 2019 / Accepted: 10 January 2020 / Published online: 18 January 2020

Abstract The naproxen adsorption capacity enhancement of activated carbon prepared from the Indian gooseberry seed-shells by manufacturing a composite blended with the surface-modified graphite powder and silver nanoparticles was studied in the present context. The composite of the nano-sized materials was prepared in dimethylformamide solution and characterized by employing XRD, Raman, EDS and FT-IR spectroscopy, FETEM, and FESEM microscopy. The pseudo-first-order, pseudo-second-order, and Elovich models were applied to test the removal kinetics. Preliminary results were also fitted to the Langmuir, Freundlich, Temkin, and Dubinine-Radushkevich (D-R) adsorption isotherm models to determine the specific parameters of each model. The effects of the initial pH of the solution, naproxen concentration, and contact time on the process were optimized. The maximum adsorption capacity was obtained as 154.98 mg g^{-1} (61.99%) with an increment of 25.31% by the addition of surface-modified graphite powder and silver nanoparticles at the optimized experimental conditions.

Keywords Activated carbon · GB-GP-AgNs composite · Naproxen removal · Adsorption kinetics and isotherms · Process optimization

Highlights • Synthesis of H_3PO_4 aided activated carbon from Indian gooseberry seed-shells (GB)
• Neem leaves extract assisted green synthesis of silver nanoparticles (AgNs)
• Adsorption capacity enhancement by adding surface-modified graphite powder and AgNs
• Kinetics and equilibrium studies on the removal of naproxen
• Maximum removal capacity of 154.98 mg g^{-1} (61.99%) with an increment of 25.31%
• Optimization by using RSM (user-defined design)

Electronic supplementary material The online version of this article (https://doi.org/10.1007/s11270-020-4411-7) contains supplementary material, which is available to authorized users.

S. Mondal (✉) · S. Patel · S. K. Majumder (✉)
Department of Chemical Engineering, Indian Institute of Technology Guwahati, Guwahati, Assam 781039, India
e-mail: somen.mondal@iitg.ac.in
e-mail: skmaju@iitg.ac.in

URL: http://www.iitg.ernet.in/chemeng/skm/home

Nomenclature

a_e	initial adsorption rate of Elovich equation (mg g^{-1} min^{-1})
b	Langmuir's adsorption affinity constant at equilibrium (dm^3 mg^{-1})
b'	Temkin isotherm constant (kJ mol^{-1})
B	Temkin adsorption isotherm constant (related to the heat of adsorption, −)
B'	Dubinine-Radushkevich (D-H) model constant (mol^2 kJ^{-2})
b_e	the extent of surface coverage for chemisorption in Elovich equation (g mg^{-1})
C_e	solution concentration at equilibrium (mg dm^{-3})
C_0	initial naproxen concentration (mg dm^{-3})
C_t	concentration of NPX in the solution (mg dm^{-3})
E	mean free energy of adsorption (kJ mol^{-1})
k_1	pseudo-first-order rate constant (min^{-1})
k_2	pseudo-second-order rate constant (g mg^{-1} min^{-1})

k_f Freundlich's constant (related to adsorption capacity, mg g^{-1})
k_t Temkin adsorption isotherm constant (equilibrium binding energy, dm^3 mg^{-1})
m adsorbent dosage (g)
n Freundlich's constant (related to adsorption intensity, −)
N number of data points (−)
q_{cal} equilibrium values obtained from the isotherm model (mg g^{-1})
q_e adsorption capacity at equilibrium (mg g^{-1})
q_{exp} equilibrium values obtained from the experiment (mg g^{-1})
Q_m maximum adsorption capacity (mg g^{-1})
q_s Dubinine-Radushkevich (D-H) model constant or adsorption capacity (mol g^{-1})
q_t adsorption capacity at time t (mg g^{-1})
R universal gas constant (kJ mol^{-1} K^{-1})
$\%R$ naproxen removal percentage (%)
T temperature (K)
t time (min)
V volume of NPX solution taken for each batch (dm^3)
ε Polanyi potential (−)

1 Introduction

Pharmaceuticals are the environmental contaminants that are widely being consumed by human beings and also by the pet animals through medicines. The unconsumed (by the body organisms), unused and rejected expired medicines, as well as the improperly treated effluents of the pharmaceutical industries, increasingly contaminated the surface water day by day. Naproxen (NPX) is one of the most conventionally accepted non-steroidal anti-inflammatory drugs. Continuous introduction of naproxen into the aquatic environment can affect the water quality and ecosystem health, which has a potential impact on drinking water supplies. Hence, the prevention acts are unavoidable to get remedy from those contaminations for environmental protection and human benefits.

Various treatment processes were utilized so far to remove that contamination from the water body. The processes like coagulation-flocculation, sedimentation, ultrasonic-degradation (Im et al. 2013), photo-degradation (Jallouli et al. 2016), bio-degradation (Marchlewicz et al. 2016; Górny et al. 2019), and the advanced oxidation were used by the researchers to eliminate the NPX from the contaminated water. The advanced oxidation processes include the uses of chlorine (Boyd et al. 2005), UV/H_2O_2 (Kim et al. 2009; Giri et al. 2011), ozone (O_3) (Giri et al. 2010; Li et al. 2019; Patel et al. 2019), along with their combinations (O_3/H_2O_2) (Uslu et al. 2012). The above processes are either not effective enough or costly or can create toxicity by producing by-products, which can provide another problem. However, adsorption of NPX by the activated carbons (ACs) attracted the attention of the researchers for its low cost and productive removal efficiency without the formation of any harmful by-products (Ilbay et al. 2015; Braghiroli et al. 2018). The adsorption efficiency of the ACs depends on the physical and chemical properties of the materials and also on the surface morphology which depends on the selection of precursor materials, the activating agent selection, activation temperature, and the heating rate (Mondal and Majumder 2019a). The ACs derived from various sources, used for the NPX adsorptions, are shown in Table 1. Some industries are already using the ACs prepared from wood or coal for effluent treatment purposes, which are costlier than the ACs from the wastes.

From the previous literature (shown in Table 1), it is clear that the studies are not sufficient or complete in that particular aspect, and a very few studies were performed for the enhancement of the NPX removal efficiency of the ACs by the addition of some foreign materials. In the present context, AC (GB) was synthesized from the Indian gooseberry seed-shells using H_3PO_4 as the activating agent. The synthesized AC showed reasonable adsorption efficiency towards NPX. The main objective of the present study is to enhance the adsorption efficiency of the prepared AC by the inclusion of some additional materials with the AC. The AC was blended with 20 wt% nano-sized surface-modified (by cetrimonium bromide, CTAB) graphite powder (GP) and 5 wt% silver nanoparticles (AgNs, synthesized following the neem-leaves extract-assisted green method) which offered the enhancement of the removal efficiency 25.31%. CTAB can cover the surface of graphite powder by positive charge, though the adsorbent surface itself becomes negatively charge but the surfactant layer on the surface takes part in the ionic interactions as the positive charge carrier. It can increase the surface bonding sites for adsorption, and also can make the adsorption medium antimicrobial.

Table 1 Adsorption of naproxen (NPX) by activated carbons (ACs) derived from various sources

Adsorbent	Adsorption capacity (mg g^{-1})	pH (−)	Time (min)	Kinetic model fitted	Isotherm model fitted	Reference
Waste apricot	106.38	5.82	60	Pseudo-second-order	Langmuir	Önal et al. (2007)
coconut shell-based granular AC	69.96	6.40	60	–	Freundlich	Yu et al. (2008)
White and black polymeric waste ACs	416.67 and 526.31	5.85	120	Pseudo-second-order	Langmuir	Sarici-Özdemir and Önal (2018)
Olive waste cakes	39.50	4.12	1800	Pseudo-second-order	Langmuir	Baccar et al. (2012)
Activated carbon (AC)	54.50	4.50	720	Pseudo-second-order	Langmuir	Hasan et al. (2012)
Raspberry carbon	47.67	3.00–5.00	1680	–	Langmuir–Freundlich	Dubey et al. (2014)
Activated carbon (AC)	54.10	7.00	240	–	Freundlich	Nam et al. (2014)
Bone char	4.28	5.00	1440	Pseudo-first-order	Langmuir	Reynel-Avila et al. (2015)
Biochar from pine chips	290.00 (N-biochar) 228.00 (O-biochar)	7.00	10,080	–	Langmuir	Jung et al. (2015)
Pine chips	290.00	7.00	10,080	Pseudo-second-order	Langmuir	Tang et al. (2015)
Magnetic AC	87.79	5.00	240	Pseudo-second-order	Langmuir	Ilbay et al. (2015)
Pine sawdust AC	325.00	6.30	5760	Pseudo-second-order	Langmuir–Freundlich (Sips)[a] and Guggenheim-Anderson-De Boer (GAB)[a]	Alvarez-Torrellas et al. (2016)
Oxidized activated carbon	80.00	5.20	720	–	Langmuir	Song et al. (2017)
Polymeric waste AC	85.00	5.85	120	–	Redlich–Peterson (R-P)[a]	Sarici-Özdemir and Önal (2018)
Prunus armeniaca stones biochar		6.00	30	Pseudo-second-order	Langmuir, Freundlich	Sekulić et al. (2018)
Activated carbon/chitosan-poly (vinyl alcohol) biocomposites	12.24	7.00	100	Pseudo-second-order	Langmuir	Saloglu and Ozcan (2018)
Softwood AC	19.20	8.20	7200	Pseudo-second-order	Freundlich	Solanki and Boyer (2019)
Magnetic chitosan/activated biochar from agricultural residues	40.82	6.00	90	–	Freundlich	Mojiri et al. (2019)
GB-GP-AgNs composite	154.98	4.40	15	Pseudo-second-order	Freundlich, D-R	present study

[a] These models are represented in Table S8

Moreover, the parametric effects (pH, initial NPX concentration, time of contact) on the adsorption process, the adsorption kinetics, and isotherms were analyzed. The AgNs has the functionalization ability depending on their sizes of diameter (Bastus et al. 2014). Hence, the AgNs, present in the GB-GP-AgNs composite, which can provide better displacement efficiency, may provide some functionalization affinity, and the catalytic activity towards the naproxen degradation/complex formation (in the Ag+ form depending on the pH values). Moreover, the conductive AgNs in the synthesized material may have antimicrobial activity (Moghayedi et al. 2017), based on the charge generated on it (Abbaszadegan et al. 2014). Hence, the present experimental composite material may be used as an efficient NPX adsorbent in the water treatment plants.

2 Experimental

2.1 Reagents and Materials

Phosphoric acid (H_3PO_4, MW = 98.0 g mol^{-1}, assay ≥ 85.0%), N, N-dimethyl formamide (DMF, MW = 73.09 g mol^{-1}, assay = 99.8%), 37.0% hydrochloric acid (HCl, MW = 36.46 g mol^{-1}, assay = 36.5–38.0%), and silver nitrate ($AgNO_3$, MW = 169.87 g mol^{-1}, assay ≥ 99.5%) of ACS reagent grade were supplied by Merck Life Science Private Limited. Caustic soda pellets (NaOH, MW = 40.00, assay = 98.0%) were bought from Himedia Laboratories Private Limited. Cetrimonium bromide (CTAB, $[(C_{16}H_{33})N(CH_3)_3]Br$, MW = 336.4 g mol^{-1}, assay = 99.0%) was purchased from Loba Chemie Pvt. Ltd. Hayman Group Limited supplied ethyl alcohol AR (C_2H_6O, MW = 46.07 g mol^{-1}, assay = 99.9%). Anhydrous naproxen ($C_{14}H_{13}O_3$, MW = 230.26 g mol^{-1}, assay = 98.5–101.5%) meets USP testing specifications and graphite powder (atomic weight = 12.01, particle size > 20 μm) supplied by Sigma-Aldrich (USA), were used in the present experiments. Milli-Q water was obtained from the Millipore synthesis unit (Model: Elix-3, Milli-Q; Make: Millipore, USA) present at the analytical laboratory, IIT Guwahati.

2.2 Activated Carbon Synthesis from Indian Gooseberry Seed-Shells

AC was prepared from Indian gooseberry (*Phyllanthus emblica*) seed-shells following a previously developed three-step chemical activation process (Mondal and Majumder 2019a, b). The gooseberries were collected from the local market near the IIT Guwahati campus, washed with milli-Q water thoroughly, peeled it out, and cut into pieces to get the seed-shells. Finally, seed-shells were dried in a hot air oven at 368 K for 7 days. In the first step, the dried seed-shells were impregnated for 18–20 h with the activating agent (50% diluted H_3PO_4 (85%) solution at a ratio of 1:4 (precursor/H_3PO_4 solution) at room temperature (303 K)). In the second step, the impregnated samples were transferred into the silica crucibles and pyrolyzed it in a muffle furnace at 773 K for 1 h, in the presence of the air atmosphere, at a heating rate of 283 K min^{-1}. In the final step, the pyrolyzed samples were activated again in the pure H_3PO_4 (85%) at 368 K for 30 min. The AC prepared from the Indian gooseberry seed-shells was then washed several times with the freshly prepared milli-Q water, and then dried it in an oven for 24 h. Then, it crashed by a mixture grinder into the nanoparticle size (< 50 μm), designated as GB (BET surface area = 1328 m^2 g^{-1}), and preserved for further analysis.

2.3 Neem Leaves Extract-Assisted Green Synthesis of Silver Nanoparticles

Thirty grams of fresh green neem (*Azadirachta indica*) leaves collected from the IIT-campus were cut into pieces and taken into 300-cm^3 milli-Q water in a 500-cm^3 glass beaker. It was heated at 353–363 K for 1 h with continuous stirring, and then filtered it to get the leaves to extract. The leaves extract was then concentrated to 200 cm^3 by boiling (yellowish-green in color), and the pH was maintained at 10.40 by the addition of 1 M NaOH solution, preserved for further use. Then, equal volume (200 cm^3) of 0.1 M $AgNO_3$ (pH 9.84) and the neem leaves extract solutions were mixed and heated for 26 h at 363 K temperature with continuous stirring (pH 10.22). The color of the solution turns black with the reduction of Ag^+ to Ag-nanoparticles (AgNs). The prepared AgNs were washed by centrifugation with milli-Q water (13,400 rpm for 20 min) several times, and finally, it dried in an oven at 423 K for 20 h and conserved for further analysis.

2.4 Preparation of the Composite Material in DMF Solution

Surface-modified graphite powder (GP, 20 wt%) and AgNs (5 wt%) were blended with nano-sized AC (GB,

75 wt%) and 200-cm^3 DMF solution was added to the mixture. The surface of the graphite powder was modified by 9.0 mM (9.0×10^{-3} mol dm^{-3}) CTAB surfactant solution before mixing. Surfactant (CTAB), which can cover the surface by positive charge, when the adsorbent surface itself becomes a negative charge, but the positive surfactant layer on the surface can take part in the ionic interactions. AFM images of graphite powder before and after the surface modification are shown in Fig. S1a and b. The surface modification procedure, in brief, has been given below in Fig. S1. The mixture was then sonicated for 2 h at 333 K and stirred it well by 1 h with the help of the magnetic stirrer at the room temperature of 303 K. Then, the DMF was drained by filtration, and the resulting composite material was washed 4–5 times with milli-Q water by centrifugation (13,400 rpm for 20 min). The prepared composite (GB-GP-AgNs) was dried in an oven at 363 K for 24 h and conserved for further analysis. The proportion of surface-modified graphite powder was selected, according to Kuwagaki (Kuwagaki et al. 2003). According to their suggestion, the addition of 20% to 30% graphite powder improves the thermal conductivity and adsorption power of the activated carbon. In addition, the improvement decreases with increasing the proportion from 20 to 30%. The BET surface area of the composite material decreased and measured as 645 m^2 g^{-1}, though the adsorption is expected to be increased due to surface functionalization.

2.5 Instrumentation

The physical properties and structure of the composite material were analyzed by the X-ray powder diffraction (XRD) (Model: D8 Advance, Make: Bruker, Netherlands) with Cu-Kα radiation of wavelength 1.5406 Å (40 kV, 40 mA) over the range of 2θ = 10–80° at a rate of 3° min^{-1}. The functional groups on the surface of the synthesized material were recognized by Fourier-transform infrared spectroscopy (FTIR) (Model: IR Affinity-1, Make: Shimadzu, Japan) using finely ground KBr with 0.5% of the sample to form pellets with the average of 30 scans ranges from 400 to 4000 cm^{-1}. The prepared sample was also characterized by a micro Raman system (Make: Horiba Jobin Yvon, Model: LabRam HR, Japan) by the diffraction of continuous monochromatic light of wavelength 488 nm with the help of G, D, and 2D band shift. Field Emission Transmission Electron Microscope (FETEM) (Make: JEOL, Model: 2100F, Japan) and Field Emission Scanning Electron Microscope (FESEM) (Make: Zeiss, Model: Sigma, Germany) were used to examine the surface morphology of the prepared sample. An Atomic Force Microscope (AFM, Make: Oxford, Model: Cipher, UK) was used to observe the surface of modified graphite powder. The composition of the prepared material was analyzed by energy-dispersive X-ray spectroscopy (EDS). High-Performance Liquid Chromatography (HPLC, Model: Prominence HPLC System; Make: Shimadzu, Singapore) was used to measure the NPX concentrations prior and after the adsorption. The digital balance (Model: ME 204, Make: Mettler Toledo, Switzerland), pH meter (Model: pH 700, Make: Eutech Instruments, Singapore), magnetic stirrer with hot plate (Make: Antech, Model: AN-MSH-680), sonicator (Model: 3.5 L/00H/DTC, Make: PCI, India), centrifuge (Model: 2-16P, Make: Sigma, Germany), hot air oven (Model: Digital, Make: SoNuu, India), and mixture grinder (Model: LLMG20 500 W, Make: Lifelong, India), were also used for the desired material synthesis purpose.

2.6 Adsorption Experiments

Naproxen adsorption was carried out in a batch mode by adding 20.0 mg of GB-GP-AgNs composite into 50-cm^3 NPX solutions in each case. The effective parameters like pH (2.40, 4.40, and 6.40 at room temperature 301 K), adsorption time (0.33–15.0 min), and naproxen concentration (25–100 mg dm^3) on the adsorption capacity were investigated. The naproxen removal percentages (*R%*), the adsorption capacities (mg g^{-1}) at equilibrium, and at time *t* were calculated by Eq. (1), Eq. (2), and Eq. (3), respectively.

$$\%R = \frac{C_0 - C_e}{C_0} \times 100 \tag{1}$$

$$q_e = \frac{V}{m}(C_0 - C_e) \tag{2}$$

$$q_t = \frac{V}{m}(C_0 - C_t) \tag{3}$$

where C_0 (mg dm^{-3}) and C_e (mg dm^{-3}) are the initial and equilibrium concentrations of naproxen in solution, respectively. q_e (mg g^{-1}) is the equilibrium adsorption

capacity. C_t (mg dm^{-3}) and q_t (mg g^{-1}) are the concentration of NPX in the solution, and adsorption capacity of the adsorbent at time t, respectively. V (dm^3) is the volume of naproxen solution taken for each batch adsorption study, and m (g) is the adsorbent (GB-GP-AgNs composite) dosage.

HPLC measured the concentration of NPX, provided with a UV detector and a C18 column (Eclipse XDB, Agilent, USA) having dimensions of 250 mm × 4.6 mm, and packed with 5-μm diameter particles. A mixture of acetonitrile (50%) and 1% aqueous solution of acetic acid (50%) was used as the mobile phase with a flow rate of 1.0 cm^3 min^{-1}. The detection wavelength and temperature were set at 260 nm and 298 K, respectively.

2.7 Adsorbent Regeneration Experiments

The used adsorbent was regenerated at room temperature with the help of pure ethyl alcohol. The used adsorbent was stirred with ethyl alcohol for 1 h using magnetic stirrer and sonicated for 30 min. Then, it was filtered, washed with ethyl alcohol, and finally was dried in a hot air oven for further use. A similar process was repeated for regeneration purposes up to the fifth recycle.

3 Results and Discussion

3.1 Material Characterization

The XRD patterns for GP, GB, AgNs, and GB-GP-AgNs are shown in Fig. 1a. The pattern for GP exhibits the sharp peak at 26.3° for (002) plane and d spacing found to be 3.36 Å. which represents the high crystallinity of GP. Two broad peaks at 25.3° and 43.5° for activated carbon obtained by gooseberry reveal the amorphous nature of GB. The visible four patterns (111), (200), (220), and (311) at 2θ for AgNs represent face-centered cubic (FCC) [JCPDS no. 01-087-0597]. The pattern for GB-GP-AgNs gives four distinguish peaks at 26.3°, 38°, 44°, 64.45°, and 77.5° for the planes (002), (111), (200), (220), and (311), respectively (Park and Jang 2003; Ghaedi et al. 2012). A sharp and intense peak at 26.3° shows the presence of a graphitic carbon plane in the composite material.

Raman spectra of GP, GB, and GB-GP-AgNs are shown in Fig. 1b, where the G band assigned for the defect in crystallinity and D band signifies the graphitic nature of the materials. GP shows the G band characteristic peak at 1536 cm^{-1} and D band at 1256.7 cm^{-1}. The low (I_D/I_G) explains the high graphitic nature. The spectrum of GB exhibits the D band at 1324.7 cm^{-1} and 1552 cm^{-1}, which are the typical spectra for carbonaceous materials (Cheng et al. 2017). A higher I_D/I_G relates to the amorphous nature of the materials. The band intensity was decreased for the composite, due to the presence of disordered and graphitic carbon material. Lower extremity also indicates the involvement of AgNs.

Figure 1 c shows the FTIR spectrum of GP, GB, AgNs, GB-GP-AgNs, and GB-GP-AgNs-AA (GB-GP-AgNs after adsorption study) which determines the functional groups present in the materials. Broad peaks at 3434 cm^{-1} and 3150 cm^{-1} correspond to the O–H bond stretching of intra-molecularly or inter-molecularly bonded alcohol. The peaks represented O–H bending of alcohol or carboxylic acid groups or S=O of sulfate or sulfonyl chlorides at 1394 cm^{-1}. The peaks represented medium C=C stretching of a conjugated alkene or cyclic alkene groups or medium N–H bending of amine groups at 1623 cm^{-1}. Peaks exhibited at 1548 cm^{-1} demonstrate the presence of active N–O stretching of nitro compounds. The peak represented medium C–N stretching of amine groups or active C–O stretching of aliphatic ester/secondary alcohol at 1111 cm^{-1}. In contrast, the peaks at 1023 cm^{-1} represent the C–N stretching of amine groups or the C–O bond stretching of vinyl or alkyl-aryl-ether. The peak at 904 cm^{-1} corresponds to the C=C bending of mono-substituted alkene groups. The peaks identified at 761 cm^{-1} are the evidence of C–H bonding of the mono-substituted, 1,2-disubstituted, 1,3-disubstituted, or 1,2,3-trisubstituted benzene derivatives. The peak represented the bond stretching of the halo compounds (C–Cl or C–Br) at 609 cm^{-1} (Dubey et al. 2014; Tang et al. 2015; Alvarez-Torrellas et al. 2016; Cheng et al. 2017; LibreTexts). After the NPX adsorption, the intensity of the peaks decreased, with some shifts or changes. The peak present in the GB-GP-AgNs composite at the wavelength 1187 cm^{-1} corresponds to the strong bond stretching of S=O of sulfate, sulfonate, or sulfonyl chloride or the C–O of ester or tertiary alcohol was shifted to the wavelength 1111 cm^{-1} after the adsorption of NPX (GB-GP-AgNs-AA). In case of GB-GP-AgNs-AA, the new peaks appeared at 1623 cm^{-1}, 1023 cm^{-1}, 761 cm^{-1}, 609 cm^{-1}. These results suggested the possibility of the ion-exchange process rather than

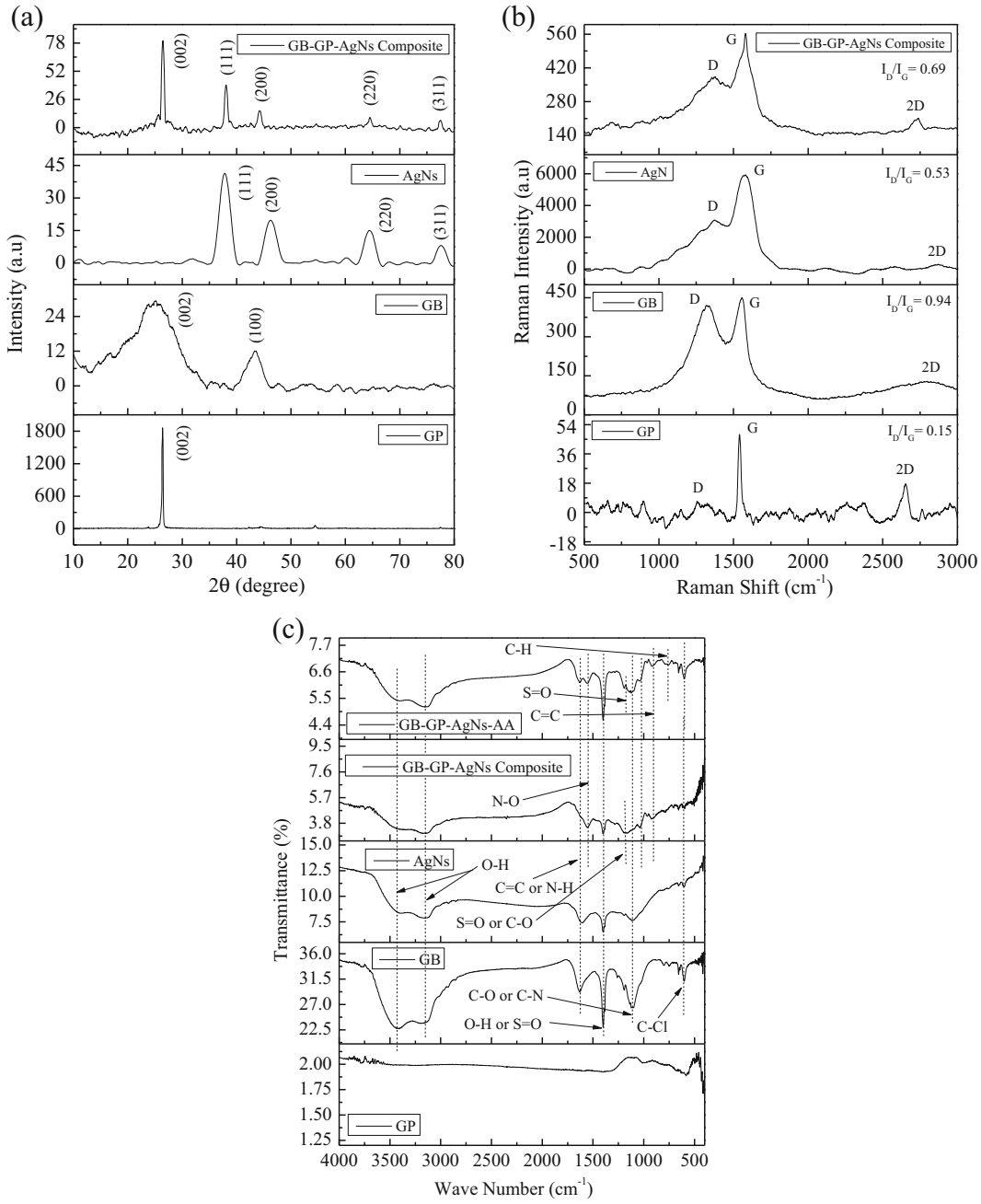

Fig. 1 **a** X-ray diffraction pattern. **b** FTIR spectra. **c** Raman spectra of GP, GB, AgNs, and the GB-GP-AgNs composite

complexation, followed by the adsorption mechanism (Blázquez et al. 2011).

From Fig. 2a particle size histogram (inset figure), average AgNs size was 13.25 nm with the polydispersity of 20.44%, whereas as per the particle size histogram of the GB-GP-AgNs composite (inset figure), the average particle size was 26.66 nm with the polydispersity of 24.23% (Fig. 2d). EDS spectrum is represented in Fig. 3f, which validates the presence of AgNs along with C and O. Figure 2 a and d represent the FETEM images of AgNs and GP-GB-AgNs composite and show the spherical shape of the particles. The AgNs and the other two components were mixed up with quite a homogeneity in the composite (Fig. 2d) (Zhang et al. 2004). In

Fig. 3b, SEAD pattern of AgNs represented the (222), (111), (200), (220), and (311) planes, which was also approved by XRD results (Fig. 1a). Figure 2 c and e represent the FESEM images of AgNs and GB-GP-AgNs composite. From Fig. 3c, it can be concluded that the AgNs were uniform in size without any aggregation (Ghaedi et al. 2012) (particle size ranges from 9 to 17 nm).

3.2 Parametric Effects on Naproxen Adsorption Capacity

3.2.1 Effect of pH on the Naproxen Adsorption Capacity

The three main interactive forces exist between the adsorbate and adsorbent molecules (a) electrostatic attractive or repulsive forces between the charged particles, (b) $\pi - \pi$ interactive forces, and (c) the H-bonding. The electrostatic forces depend mainly on the surface charges, which depend on the pH values. Hence, the pH of the solutions plays a prominent role in the adsorption mechanism. The effect of pH on the NPX removal using GB-GP-AgNs composite was studied at the pH values of 2.40, 4.40, and 6.40. HCl and NaOH solutions of 1 M were added to maintain the acidity and basicity of the solutions, respectively. The removal efficiency was higher at

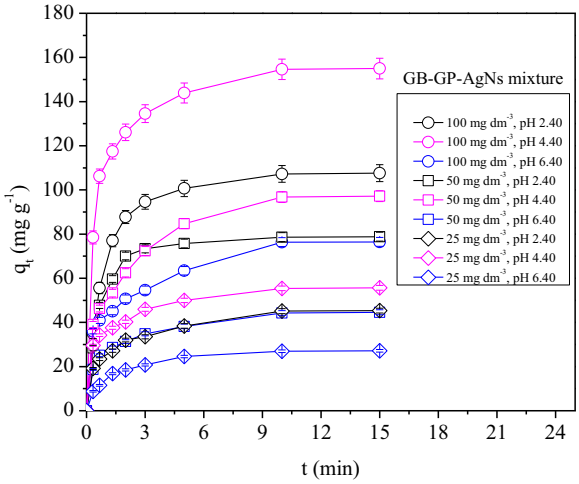

Fig. 3 Variations of adsorption capacities of GB-GP-AgNs composite concerning time depending on the pHs and the initial NPX concentrations

pH 4.40 than the highly acidic (pH 2.40) and slightly basic (pH 6.40) conditions (Fig. 3). Such adsorption nature may depend on the point of zero charges (PZCs) of the experimental composite material (pH_{pzc} ~ 5.69) and the ionization form of naproxen (pKa ~ 4.2). The pH-drift method was used to measure the pH_{pzc} point. In this method, 500 cm^3 of 0.01 M NaCl solution was taken in a constant temperature (298 K)

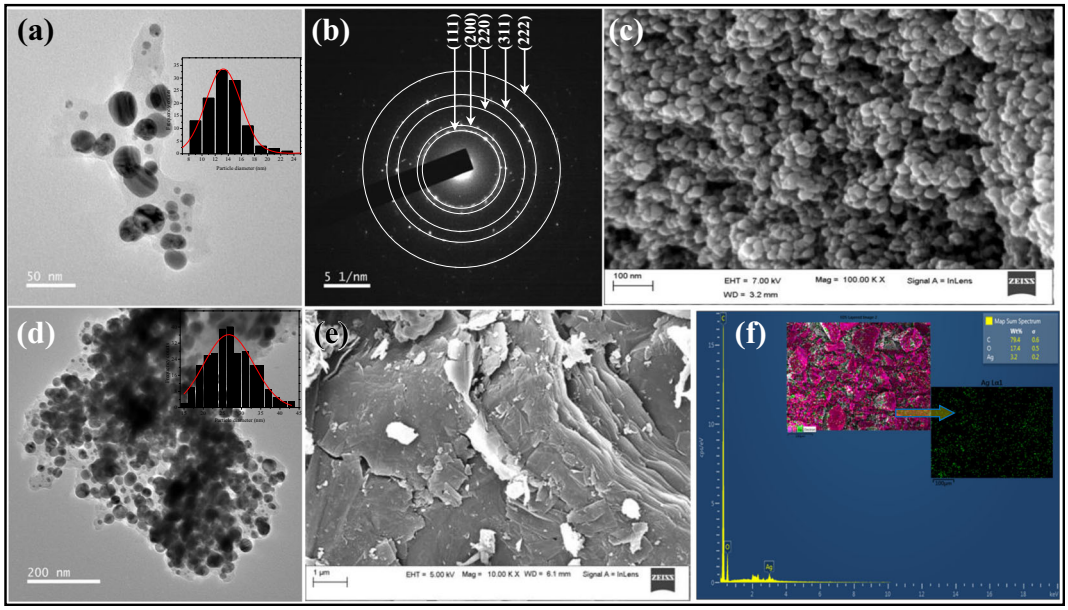

Fig. 2 **a** FETEM micrograph of AgNs and particle size histogram (inset figure). **b** SEAD pattern of AgNs. **c** FESEM image of AgNs. **d** FETEM micrograph of GB-GP-AgNs composite and particle size histogram (inset figure). **e** FESEM image of GB-GP-AgNs composite. **f** EDS spectrum and EDS mapping (inset figure) of GB-GP-AgNs composite

titration vessel. The dissolved gases were removed from the solution by nitrogen bubbling, and the pH was maintained to a continuous value between 2 and 8. Then, 0.10-g GB-GP-AgNs composite was added to the solution, and the suspension was stirred for 1 h to attain the equilibrium. The final pH values were measured and plotted against the initial pH values.

The pH at which the curve crossed the diagonal line, $pH_{initial} = pH_{final}$, was taken as the point of zero charges (PZCs), demonstrated in Fig. 4. Dubey et al. (2014) reported the pH_{pzc} value of 5.48, for Raspberry derived carbon, and Newcombe (Newcombe et al. 1993), obtained the value of 6.02 for the granular activated carbon. According to the pKa value of NPX, at pH > 4.2, ionization of NPX led to form anions. Additionally, at pH < 4.2, the adsorbent surface behaves as positively charged, and at pH > 6, the adsorbent surface behaves as negatively charged (Nodeh et al. 2018). Thus, the high electrostatic interactive forces between the positively charged adsorbent surfaces and the negatively charged naproxen anions followed the high adsorption capacity towards NPX at pH 4.40. At pH < 4.2, the ionic interaction is not possible, and at pH > 6, the electrostatic repulsive force between the naproxen anions and negatively charged surfaces of the adsorbent diminishes the adsorption capacity. Moreover, with decreasing pH values from 6.40 to 2.40, the AgNs turned into Ag^+ from which also can take part in NPX adsorption or removal.

The highest adsorption capacity of 154.98 mg g^{-1} was obtained at pH 4.40, considered as the optimum pH value. The variations of adsorption capacities of the activated carbon (GB) were also experimented for 100 mg dm^{-3}, 50 mg dm^{-3}, and 25 mg dm^{-3} solutions with 20.0 mg dose at the optimized pH value of 4.40 and demonstrated in Fig. 5. GB followed the similar trend for the adsorption capacity; however, it held a lower value of maximum 123.68 mg g^{-1}. Hence, it was observed from Figs. 3 and 5 that the addition of 20 wt% GP and 5 wt% AgNs increases the adsorption capacity of GB 25.31% (123.68 mg g^{-1} to 154.98 mg g^{-1}).

3.2.2 *Effect of the Initial Naproxen Concentration on the Adsorption Capacity*

The impact of initial concentrations on the adsorption capacities was measured using 100 mg dm^{-3}, 50 mg dm^{-3}, and 25 mg dm^{-3} NPX solutions at room temperature (301 K) for a fixed adsorbent dose (20.0 mg per 50 cm^3). At a constant pH value, the adsorption capacities were increased with the increase of initial NPX concentrations, probably due to the availability of more NPX anions for adsorption before reaching the surface saturation point (Fig. 3). Beyond the saturation point, the adsorption capacity remained constant; no further change in the adsorption capacity was found to occur even if the initial concentration was increased. At the present experimental condition, 100 mg dm^{-3} showed a higher adsorption capacity of 154.98 mg g^{-1} at a pH value of 4.40.

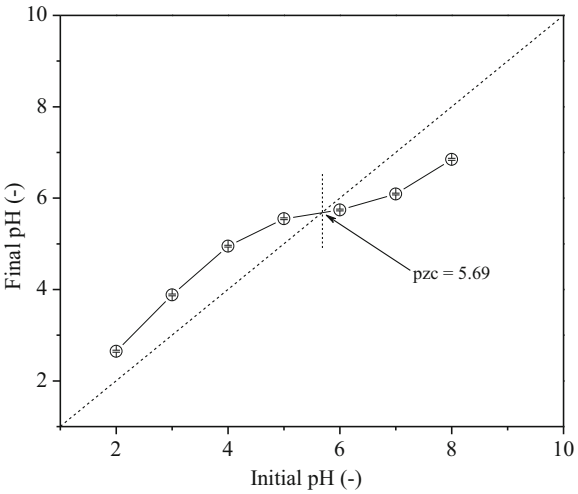

Fig. 4 Determination of the PZC of GB-GP-AgNs composite using the pH-drift method

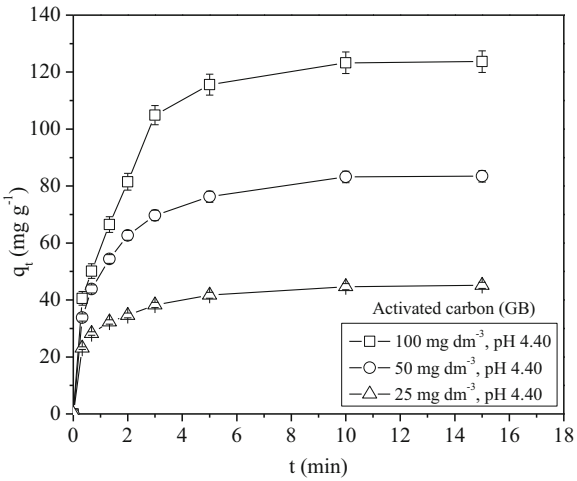

Fig. 5 Variations of adsorption capacities of GB concerning time depending on the initial NPX concentrations

3.2.3 Effect of the Contact Time on the Naproxen Adsorption Capacity

It was observed that with the increase of contact time, the physical adsorption capacity of the adsorbent increases. In the presence of ionic interactions between the surfaces of the adsorbent and the adsorbate ions, the adsorption process becomes faster. The effect of contact time on the adsorption capacity was examined by adding 20.0 mg of GB-GP-AgNs composite into 50-cm^3 aqueous solution of NPX (for a fixed pH value at different NPX concentrations and vice versa) and testing the samples at 0.33 min to 15 min time intervals (Fig. 3). The removal efficiency reached to 31.40% within 0.33 min and increased to 61.99% in 10–15 min for 100 mg dm^{-3} concentration at a pH value of 4.40. Initially, the rapid adsorption rate on the adsorbent surface was observed, due to the presence of ionic interactions between the oppositely charged adsorbent surface and the adsorbate ions. Within 10 min to 15 min, the removal capacities were not changed significantly attaining the equilibrium (Fig. 3). Therefore, 15 min can be considered as the equilibrium time for further adsorption studies.

3.3 Adsorption Kinetics

Pseudo-first-order, pseudo-second-order, and Elovich models were studied to determine the kinetic parameters of the NPX adsorption, at the previous optimized results (equilibrium contact time, 15 min; the adsorbent dose, 20.0 mg, and initial NPX concentrations, 100 mg dm^{-3}) as demonstrated in Fig. 3, with the variation of pH values from 2.40 to 6.40. Linearized pseudo-first-order model can be represented by Eq. (4) (Baccar et al. 2012; Alvarez-Torrellas et al. 2016).

$$\log(q_e - q_t) = \log q_e - \frac{k_1 t}{2.303} \tag{4}$$

where q_e and q_t are the amount of NPX adsorbed (mg g^{-1}) at equilibrium and at time t. k_1 (min^{-1}) is the first-order rate constant, obtained from the plot of $log\ (q_e - q_t)$ vs. t (min) (Fig. 6a). The pseudo-second-order kinetic model is represented by Eq. (5) (Baccar et al. 2012; Alvarez-Torrellas et al. 2016).

$$\frac{t}{q_t} = \frac{1}{k_2 q_e^2} + \frac{t}{q_e} \tag{5}$$

The pseudo-second-order rate constants k_2 (g mg^{-1} min^{-1}) and q_e are the intercept and slope of the t/q_t vs. t plot (Fig. 6b). The intra-particle diffusion model is not interpreted in the present context as it can be applied within very restrictive conditions such as adsorption in a semi-infinite solid and constant liquid phase concentration in the absence of external mass transfer resistance (Schwaab et al. 2017). The Elovich equation, which is used to demonstrate the matter of the chemical adsorption processes on the different surfaces, is expressed in the linearized form by Eq. (6) (Baccar et al. 2012; Alvarez-Torrellas et al. 2016).

$$q_t = \frac{\ln(a_e b_e)}{b_e} + \frac{1}{b_e} \ln t \tag{6}$$

where a_e and b_e represent the initial adsorption rate (mg g^{-1} min^{-1}) and the extent of the surface coverage utilized for the chemisorption (g mg^{-1}) or the activation energy required for chemisorption. The values of a_e and b_e can be determined from the q_t vs. lnt plot (Fig. 6c). The average relative errors ($ARE\%$), the deviation between the experimental and the kinetic and isotherm models data were calculated by using Eq. (7).

$$ARE(\%) = \frac{100}{N} \sum_{1}^{N} \left| \frac{q_{cal} - q_{\exp}}{q_{\exp}} \right| \tag{7}$$

where q_{exp} and q_{cal} (mg g^{-1}) represent the values of experimental and calculated equilibrium adsorption capacities, and N represents the number of data points. The parameters obtained from the kinetic models are tabulated in Table 2.

In comparison with the pseudo-first-order model, the pseudo-second-order model satisfied the experimental data very well with the lower $ARE\%$ at all pH values. The q_e value at the pH 4.40 (156.01 mg g^{-1}) was only 0.66% higher than the experimental equilibrium value (154.98 mg g^{-1}), and the q_t values deviate with the low $ARE\%$ of 3.95. The a_e values of the Elovich model were high enough to satisfy the kinetic data demonstrated in Fig. 5. In the meantime, the much lower values of b_e (Table 2, lowest $b_e = 0.044$ for pH 4.40) give the evidence of good adsorption and effective π–π interaction between the adsorbent and adsorbate surfaces (Zhao et al. 2011; Umbreen et al. 2018). Moreover, at

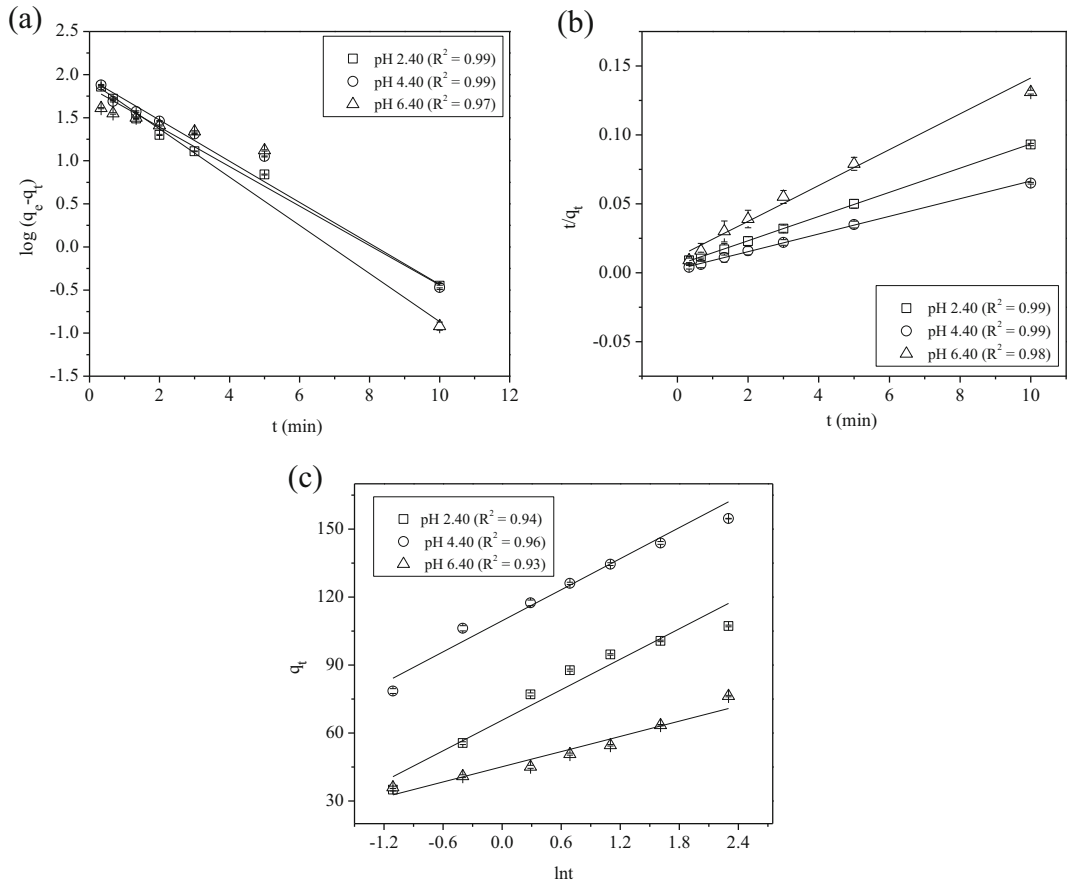

Fig. 6 NPX adsorption kinetics: **a** pseudo-first-order model, **b** pseudo-second-order model, and **c** Elovich model

pH 4.40, the Elovich model showed a higher determination coefficient value of $R^2 = 0.98$, and the q_t values deviate with the very low *ARE%* of 2.73. This ensures the presence of some chemical type of interactions. Hence, the leading process is chemisorption or ion exchange, as reported in the previous studies for the metal ion adsorption on activated carbon (Demirbas et al. 2009). Sample calculations of the kinetic models are represented in Table S1 (pseudo-first-order), Table S2 (pseudo-second-order), and Table S3 (Elovich).

Table 2 Kinetic parameters for the NPX adsorption onto the GB-GP-AgNs composite material (NPX concentration, 100 mg dm^{-3}; the volume of NPX solution, 50 cm^3; GB-GP-AgNs dose, 20.0 mg; temperature, 301 K and contact time, 0.33–15 min)

Kinetic models	pH	Kinetic parameters		R^2	*ARE%*
Pseudo-first-order	2.40	$k_1 = 0.53$	$q_e = 70.83$	0.99	48.58
	4.40	$k_1 = 0.55$	$q_e = 88.87$	0.99	57.28
	6.40	$k_1 = 0.64$	$q_e = 84.76$	0.97	26.24
Pseudo-second-order	2.40	$k_2 = 0.014$	$q_e = 114.03$	0.99	4.96
	4.40	$k_2 = 0.013$	$q_e = 156.01$	0.99	3.95
	6.40	$k_2 = 0.016$	$q_e = 77.04$	0.98	13.23
Elovich	2.40	$a_e = 417.92$	$b_e = 0.048$	0.94	6.76
	4.40	$a_e = 2758.48$	$b_e = 0.044$	0.96	2.73
	6.40	$a_e = 629.45$	$b_e = 0.089$	0.93	4.90

3.4 Adsorption Isotherm

Langmuir, Freundlich, Temkin, and Dubinine-Radushkevich (D-R) adsorption isotherm models were studied (pH range, 2.40–6.40; the volume of NPX solution, 50 cm^3; NPX concentrations, 25–100 mg dm^{-3}; contact time, 15 min, and the adsorbent dose, 20.0 mg). The Langmuir adsorption model, relevant for the monolayer adsorption on the uniform adsorbent surfaces, can be expressed as (Hasan et al. 2012; Alvarez-Torrellas et al. 2016)

$$\frac{C_e}{q_e} = \frac{1}{bQ_m} + \frac{C_e}{Q_m} \tag{8}$$

The adsorption coefficients b (dm^3 mg^{-1}) and Q_m (mg g^{-1}) are the equilibrium adsorption affinity constant and the maximum adsorption capacity, estimated from the C_e/q_e vs. C_e plot (Fig. 7a). Freundlich isotherm, represented by Eq. (9), describes the adsorption on the various surfaces (Baccar et al. 2012; Hasan et al. 2012).

$$\log q_e = \log k_f + \frac{1}{n}\log C_e \tag{9}$$

where k_f (mg g^{-1}) and n represent the adsorption capacity and its intensity, obtained from the intercept and slope of $log\ q_e$ vs. $log\ C_e$ plot (Fig. 7b). The interactions between the adsorbate and the adsorbent molecules are characterized by the Temkin isotherm model, which can be expressed by Eq. (10) (Demirbas et al. 2009; Ghaedi et al. 2012).

$$q_e = B\ln k_t + B\ln C_e \tag{10}$$

where k_t is related to the equilibrium binding energy (dm^3 mg^{-1}) and $B = \frac{RT}{b}$is associated with the heat of

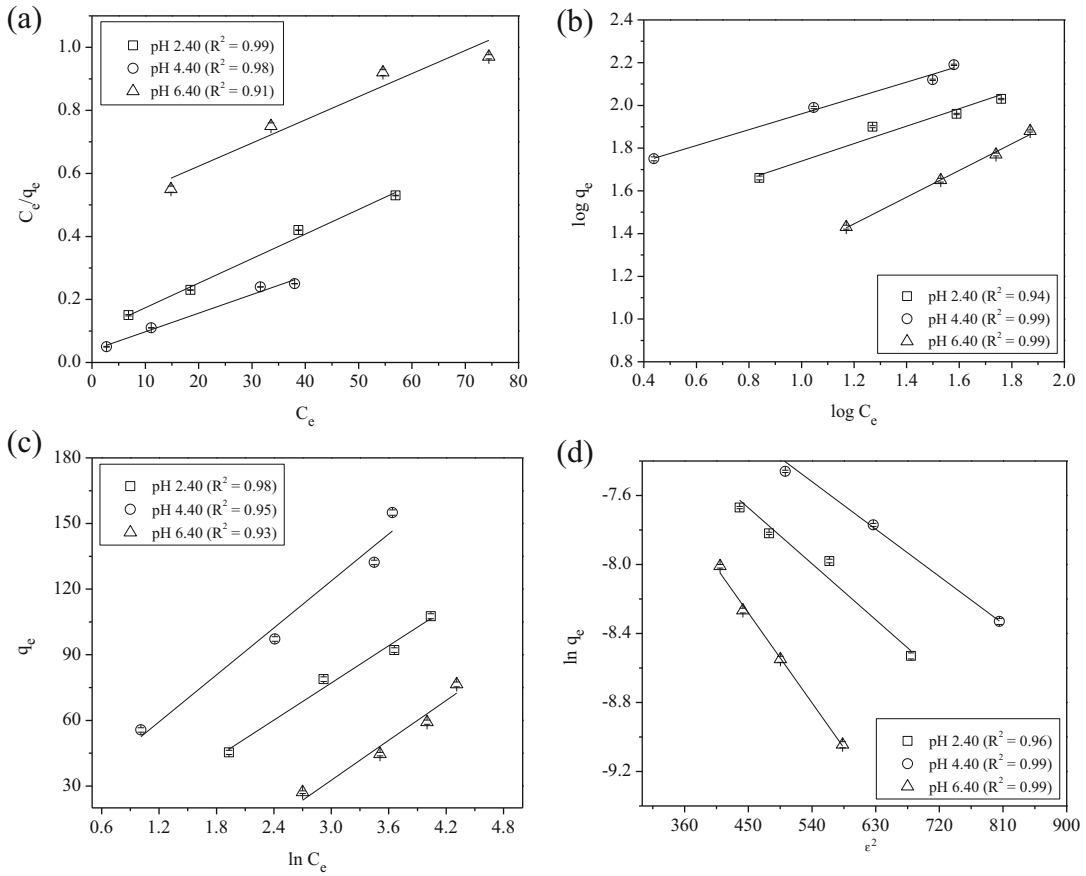

Fig. 7 Adsorption isotherms: **a** Langmuir, **b** Freundlich, **c** Temkin, and **d** Dubinine-Radushkevich (D-R)

Table 3 Adsorption isotherm constants for the sorption of NPX onto the GB-GP-AgNs composite material (NPX concentrations, 25, 50, 75, and 100 mg dm^{-3}; the volume of NPX solution, 50 cm^3; GB-GP-AgNs dose, 20.0 mg; temperature, 301 K and contact time, 15 min)

Isotherms	pH	Constants			R^2	*ARE%*
Langmuir	2.0	$Q_m = 128.21$	$b = 0.082$		0.99	2.89
	4.40	$Q_m = 169.49$	$b = 0.154$		0.98	8.15
	6.40	$Q_m = 136.05$	$b = 0.015$		0.91	5.22
Freundlich	2.40	$k_f = 21.36$	$n = 2.44$		0.94	1.28
	4.40	$k_f = 38.88$	$n = 2.70$		0.99	0.68
	6.40	$k_f = 4.99$	$n = 1.60$		0.99	0.48
Temkin	2.40	$B = 28.27$	$K_t = 0.76$		0.98	3.30
	4.40	$B = 35.79$	$K_t = 1.58$		0.95	5.62
	6.40	$B = 30.38$	$K_t = 0.15$		0.93	8.43
D-R	2.40	$q_s = 0.0024$	$B' = 0.0036$	$E = 11.77$	0.96	5.40
	4.40	$q_s = 0.0028$	$B' = 0.0031$	$E = 12.80$	0.99	2.77
	6.40	$q_s = 0.0034$	$B' = 0.0058$	$E = 9.28$	0.99	3.38

adsorption. R is the molar gas constant (8.314×10^{-3} kJ mol^{-1} K^{-1}), T is the absolute temperature in K, and b' is the Temkin isotherm constant in kJ mol^{-1}. The Temkin isotherm constants can be obtained from the q_e vs. $ln\ C_e$ plot (Fig. 7c). The linear form of the D-R model (used to analyze the adsorption processes on the various surfaces when the binding sites acquire different potentials) is represented by Eq. (11) (Nodeh et al. 2018; Sarici-Özdemir and Önal 2018).

$$\ln q_e = \ln q_s - B' \varepsilon^2 \tag{11}$$

where q_s and q_e represent the adsorption capacity (mol g^{-1}) and the equilibrium NPX concentration on the adsorbent surface (mol g^{-1}). The constants of the model, q_s, and B' (mol^2 kJ^{-2}) can be estimated from the lnq_e vs. ε^2 plot (Fig. 7d). Polanyi potential (ε) is related to the equilibrium concentration and expressed by Eq. (12).

$$\varepsilon = RT \ln\left(1 + \frac{1}{C_e}\right) \tag{12}$$

C_e is the equilibrium NPX concentration in the solution (mol dm^{-3}). The mean adsorptive free energy (E) is calculated by Eq. (13).

$$E = {}^{1}\Big/\sqrt{2B'} \tag{13}$$

Figure 7 represents the isotherm models, and Table 3 represents the isotherm constants, which indicate that the adsorption isotherm changed with the change in pH values.

Through the values of the determination, coefficients were high, the Langmuir monolayer adsorption capacity showed very high deviation from the

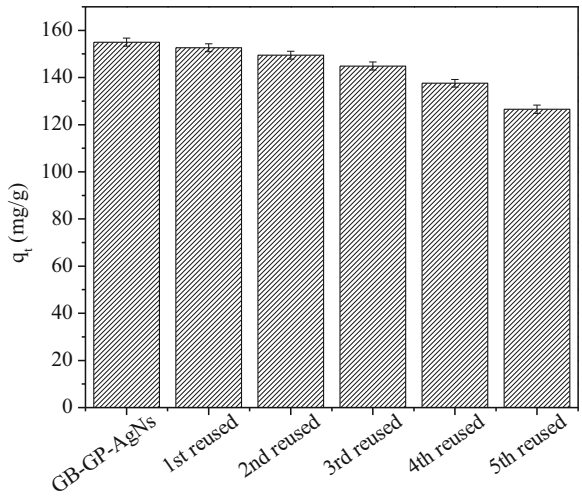

Fig. 8 Effect of recycling numbers on the adsorbed amount of NPX over GB-GP-AgNs composite (pH: 4.40, adsorption time: 15 min and initial concentration of NPX: 100 mg dm^{-3})

experimental data. Hence, it was assumed that the Freundlich isotherm model may satisfy the experimental data. The constant k_f, which is related to the tendency of the adsorbent to adsorb ranges from 4.99 to 38.88 mg g^{-1} and n, which represents the potentiality hold the values > 1 in all the cases. At the pH value of 4.40, the k_f and n acquired the highest value with the low *ARE%* of 0.68. The q_e value calculated at that pH was 151.36 mg g^{-1}, 2.34% lower than our experimental q_e value (154.98 mg g^{-1}). Therefore, the Freundlich isotherm model indicates the favorable multilayered adsorption on the heterogeneous surfaces of the adsorbent (Blázquez et al. 2011; Saadi et al. 2015). The positive values of the Temkin constant B (maximum 35.79, at the pH 4.40) obtained in the present experimentation demonstrated the adsorption process as an endothermic one, which provides the affirmation of chemical or ionic interaction rather than the physical adsorption (Inam et al. 2017). The D–R isotherm model analyzed the mean free energy (E) required for the adsorption process along with the type of adsorption. The free energy, $E <$ 8 kJ mol^{-1}, is responsible for the physical adsorption process, but when 8 kJ $mol^{-1} < E <$ 16 kJ mol^{-1}, ion exchange is the governing factor. Adsorption is governed by particle diffusion when $E > 16$ kJ mol^{-1} (Argun et al. 2007). As shown in Table 3, the E values varied from 9.28 to 12.80 (at pH 4.40), signified that the adsorption process followed the chemical or ion-exchange type of mechanism. Maximum E (12.80 kJ mol^{-1}) and minimum B' (0.0031 mol^2 kJ^{-2}, related to the activation energy required for the adsorption process) values at the pH 4.40, provide a pleasant correspondence with the chemical or ion-exchange route of adsorption. Sample calculations of the Langmuir, Freundlich, Temkin, and Elovich isotherm models are shown in Table S4, Table S5, Table S6, and Table S7, respectively.

The higher determination coefficients for Langmuir isotherm and the pseudo-second-order kinetic model recommend the bond formation between the NPX anions and the positively charged groups; however, the high determination coefficients of Freundlich isotherm support more than one mechanism and a degree of heterogeneity. Therefore, from the experimental results, it was difficult to suggest a particular mechanism that occurred in the present case.

3.5 Adsorbent Regeneration Study

The spent adsorbent (used at pH 4.40, NPX concentration 100 mg dm^{-3} and adsorption time 15 min) was regenerated by washing with ethyl alcohol and reused it again for the adsorptive removal of NPX. As shown in Fig. 8, the adsorption capacities of GB-GP-AgNs composite towards NPX (100 mg dm^{-3}) decreased a little with the increasing number of recycles. However, the adsorption capacity decreased only 18.32% (28.39 mg dm^{-3}) after the fifth cycle, which demonstrated its possible application as a suitable adsorbent in commercial plants.

4 Conclusion

The proposed composite material (GB-GP-AgNs) showed an excellent NPX removal capacity of 61.99% from the 100 mg dm^{-3} contaminated solution at pH 4.40. The adsorption capacity of GB was increased 25.31% by the addition of only 20 wt% surface-modified graphite powder and 5 wt% AgNs. The highly pH-dependent removal process showed the adsorption capacity (maximum) of 154.98 mg g^{-1} at pH 4.40 with the initial NPX concentration of 100 mg dm^{-3}. Experimental data were best fitted with the pseudo-second-order kinetic model and somewhat with the Elovich model, indicated chemical/ion-exchange type of adsorption at the optimum pH value of 4.40. The suitability of the kinetic models except for the pseudo-second-order was changed with the change of pH values. Freundlich isotherm satisfied the experimental data better than the Langmuir isotherm, indicated that the multilayer adsorption occurred on the various surfaces of the adsorbent. The chemical or ion-exchange type of adsorption again suggested from the higher free energy (E = 12.80 kJ mol^{-1}) and lower activation energy (B' = 0.0031) values for the D-R adsorption isotherm at pH 4.40. The reduced quadratic model well explained the parametric optimization results from the experiments under the user-defined discrete design of RSM. Further study required as the mechanism of the NPX adsorption was very complex and not possible to define exactly. However, from the present study, it can be concluded that the GB-GP-AgNs composite can be used as an efficient and good recyclable NPX adsorbent.

Acknowledgments The authors are grateful to the Analytical Laboratory, Department of Chemical Engineering and Central

Instrument Facility, Indian Institute of Technology Guwahati, for the assistance and support to perform the necessary analysis.

Funding Information The Department of Science and Technology (Water Technology Initiative), Government of India, provided financial support of this work, through the Grant Number: DST/TM/WTI/2K16/20 (C)-A, dated March 3, 2017.

Compliance with Ethical Standards

Conflict of Interest The authors declare that there is no conflict of interest.

References

Abbaszadegan, A., Ghahramani, Y., Gholami, A., Hemmateenejad, B., Dorostkar, S., Nabavizadeh, M., & Sharghi, H. (2014). The effect of charge at the surface of silver nanoparticles on antimicrobial activity against gram-positive and gram-negative bacteria: A preliminary study. *Journal of Nanomaterials, 2015*, 1–8.

Alvarez-Torrellas, S., Munoz, M., Zazo, J. A., Casas, J. A., & García, J. (2016). Synthesis of high surface area carbon adsorbents prepared from pine sawdust-Onopordum acanthium L. for nonsteroidal anti-inflammatory drug adsorption. *Journal of Environmental Management, 183*, 294–305.

Argun, M. E., Dursun, S., Ozdemir, C., & Karatas, M. (2007). Heavy metal adsorption by modified oak sawdust: Thermodynamics and kinetics. *Journal of Hazardous Materials, 141*, 77–85.

Baccar, R., Sarrà, M., Bouzid, J., Feki, M., & Blánquez, P. (2012). Removal of pharmaceutical compounds by activated carbon prepared from the agricultural by-product. *Chemical Engineering Journal, 211*, 310–317.

Bastus, N. G., Merkoci, F., Piella, J., & Puntes, V. (2014). Synthesis of highly monodisperse citrate stabilized silver nanoparticles of up to 200 nm: Kinetic control and catalytic properties. *Chemistry of Materials, 26*, 2836–2846.

Blázquez, G., Martín-Lara, M. A., Tenorio, G., & Calero, M. (2011). Batch biosorption of lead(II) from aqueous solutions by olive tree pruning waste: Equilibrium, kinetics, and thermodynamic study. *Chemical Engineering Journal, 168*, 170–177.

Boyd, G., Zhang, S., & Grim, D. (2005). Naproxen removal from water by chlorination and biofilm processes. *Water Research, 39*, 668–676.

Braghiroli, F. L., Bouafif, H., Neculita, C. M., & Koubaa, A. (2018). Activated biochar as an effective sorbent for organic and inorganic contaminants in water. *Water Air, and Soil Pollution, 229*, 230.

Cheng, S., Zhang, L., Xia, H., & Peng, J. (2017). Characterization and adsorption properties of La and Fe modified activated carbon for dye wastewater treatment. *Green Processing and Synthesis, 6*, 487–498.

Demirbas, E., Dizge, N., Sulak, M. T., & Kobya, M. (2009). Adsorption kinetics and equilibrium of copper from aqueous solutions using hazelnut shell activated carbon. *Chemical Engineering Journal, 148*, 480–487.

Dubey, S. P., Dwivedi, A. D., Lee, C., Kwon, Y. N., Sillanpaa, M., & Ma, L. Q. (2014). Raspberry derived mesoporous carbon-tubules and fixed-bed adsorption of pharmaceutical drugs. *Journal of Industrial & Engineering Chemistry, 20*, 1126–1132.

Ghaedi, M., Sadeghian, B., Pebdani, A. A., Sahraei, R., Daneshfar, A., & Duran, C. (2012). Kinetics, thermodynamics and equilibrium evaluation of direct yellow 12 removal by adsorption onto silver nanoparticles loaded activated carbon. *Chemical Engineering Journal, 187*, 133–141.

Giri, R. R., Ozaki, H., Ota, S., Takanami, R., & Taniguchi, S. (2010). Degradation of common pharmaceuticals and personal care products in mixed solutions by advanced oxidation techniques. *International Journal of Environmental Science and Technology, 7*, 251–260.

Giri, R. R., Ozaki, H., Takayanagi, Y., Taniguchi, S., & Takanami, R. (2011). Efficacy of ultraviolet radiation and hydrogen peroxide oxidation to eliminate large number of pharmaceutical compounds in mixed solution. *International Journal of Environmental Science and Technology, 8*, 19–30.

Górny, D., Guzik, U., Hupert-Kocurek, K., & Wojcieszynska, D. (2019). Naproxen ecotoxicity and biodegradation by bacillus thuringiensis B1(2015b) strain. *Ecotoxicology and Environmental Safety, 167*, 505–512.

Hasan, Z., Jeon, J., & Jhung, S. H. (2012). Adsorptive removal of naproxen and clofibric acid from water using metal-organic frameworks. *Journal of Hazardous Materials, 209-210*, 151–157.

Ilbay, Z., Sahin, S., Kerkez, O., & Bayazit, S. S. (2015). Isolation of naproxen from wastewater using carbon-based magnetic adsorbents. *International Journal of Environmental Science and Technology, 12*, 3541–3550.

Im, J. K., Heo, J., Boateng, L. K., Her, N., Flora, J. R., Yoon, J., Zoh, K. D., & Yoon, Y. (2013). Ultrasonic degradation of acetaminophen and naproxen in the presence of single-walled carbon nanotubes. *Journal of Hazardous Materials, 254–255*, 284–292.

Inam, E., Etim, U. J., Akpabio, E. G., & Umoren, S. A. (2017). Process optimization for the application of carbon from plantain peels in dye abstraction. *Journal of Taibah University for Science, 11*, 173–185.

Jallouli, N., Elghniji, K., Hentati, O., Ribeiro, A. R., Silva, A. M. T., & Ksibi, M. (2016). UV and solar photo-degradation of naproxen: TiO_2 catalyst effect, reaction kinetics, products identification, and toxicity assessment. *Journal of Hazardous Materials, 304*, 329–336.

Jung, C., Boateng, L. K., Flora, J. R. V., Oh, J., Braswell, M. C., Son, A., & Yoon, Y. (2015). Competitive adsorption of selected non-steroidal anti-inflammatory drugs on activated biochars: Experimental and molecular modeling study. *Chemical Engineering Journal, 264*, 1–9.

Kim, I., Yamashita, N., & Tanaka, H. (2009). Performance of UV and UV/H_2O_2 processes for the removal of pharmaceuticals detected in secondary effluent of a sewage treatment plant in Japan. *Journal of Hazardous Materials, 166*, 1134–1140.

Kuwagaki, H., Meguro, T., Tatami, J., Komeya, K., & Tamura, K. (2003). An improvement of thermal conduction of activated carbon by adding graphite. *Journal of Materials Science, 38*, 3279–3284.

Li, M., Chen, Z., Wang, Z., & Wen, Q. (2019). Investigation on degradation behavior of dissolved effluent organic matter, organic micro-pollutants and bio-toxicity reduction from

secondary effluent treated by ozonation. *Chemosphere, 217*, 223–231.

Marchlewicz, A., Domaradzka, D., Guzik, U., & Wojcieszyńska, D. (2016). *Bacillus thuringiensis* B1 (2015b) is a gram-positive Bacteria able to degrade naproxen and ibuprofen. *Water, Air, and Soil Pollution, 227*, 197.

Moghayedi, M., Goharshadi, E. K., Ghazvini, K., Ahmadzadeh, H., Ranjbaran, L., Masoudi, R., & Ludwig, R. (2017). Kinetics and mechanism of antibacterial activity and cytotoxicity of Ag-RGO nanocomposite. *Colloids and Surfaces B, 159*, 366–374.

Mojiri, A., Kazeroon, R. A., & Gholami, A. (2019). Cross-linked magnetic chitosan/activated biochar for removal of emerging micropollutants from water: Optimization by the artificial neural network. *Water, 11*, 1–18.

Mondal, S., & Majumder, S. K. (2019a). Synthesis of phosphate functionalized highly porous activated carbon and its utilization as an efficient copper (II) adsorbent. *Korean Journal of Chemical Engineering, 36*, 701–712.

Mondal, S., & Majumder, S. K. (2019**b**). Honeycomb-like porous activated carbon for efficient copper (II) adsorption synthesized from natural source: Kinetic study and equilibrium isotherm analysis. *Journal of Environmental Chemical Engineering, 7*, 103236.

Nam, S. W., Choi, D. J., Kim, S. K., Her, N., & Zoh, K. D. (2014). Adsorption characteristics of selected hydrophilic and hydrophobic micropollutants in water using activated carbon. *Journal of Hazardous Materials, 270*, 144–152.

Newcombe, G., Hayes, R., & Drikas, M. (1993). Granular activated carbon: Importance of surface properties in the adsorption of naturally occurring organics. *Colloids and Surfaces, A: Physicochemical and Engineering Aspects, 78*, 65–71.

Nodeh, M. K. M., Radfard, M., Ali, Z. L., & Nodeh, H. R. (2018). Enhanced removal of naproxen from wastewater using silica magnetic nanoparticles decorated onto graphene oxide; parametric and equilibrium study. *Separation Science and Technology, 53*, 2476–2485.

Önal, Y., Akmil-Başar, Ç. & Sarıcı-Özdemir, Ç. (2007). Elucidation of the naproxen sodium adsorption onto activated carbon prepared from waste apricot: Kinetic, equilibrium and thermodynamic characterization. *Journal of Hazardous Materials, 148*, 727–734.

Park, S. J., & Jang, Y. S. (2003). Preparation and characterization of activated carbon fibers supported with silver metal for antibacterial behavior. *Journal of Colloid and Interface Science, 261*, 238–243.

Patel, S., Majumder, S. K., Das, P., & Ghosh, P. (2019). Ozone microbubble-aided intensification of degradation of naproxen in a plant prototype. *Journal of Environmental Chemical Engineering, 7*, 103102.

Reynel-Avila, H. E., Mendoza-Castillo, D. I., Bonilla-Petriciolet, A., & Silvestre-Albero, J. (2015). Assessment of naproxen adsorption on bone char in aqueous solutions using batch and fixed-bed processes. *Journal of Molecular Liquids, 209*, 187–195.

Saadi, R., Saadi, Z., Fazaeli, R., & Fard, N. E. (2015). Monolayer and multilayer adsorption isotherm models for sorption from aqueous media. *Korean Journal of Chemical Engineering, 32*, 787–799.

Saloglu, D., & Ozcan, N. (2018). Activated carbon embedded chitosan/polyvinyl alcohol biocomposites for adsorption of nonsteroidal anti-inflammatory drug-naproxen from wastewater. *Desalination and Water Treatment, 107*, 72–84.

Sarici-Özdemir, C., & Önal, Y. (2018). Study to observe the applicability of the adsorption isotherms used for the adsorption of medicine organics onto activated carbon. *Particulate Science and Technology, 36*, 254–261.

Schwaab, M., Steffani, E., Barbosa-Coutinho, E., & Júnior, J. B. S. (2017). Critical analysis of adsorption/diffusion modelling as a function of time square root. *Chemical Engineering Science, 173*, 179–186.

Sekulić, M. T., Pap, S., Stojanović, Z., Bošković, N., Radonić, J., & Knudsen, T. S. (2018). Efficient removal of priority, hazardous priority and emerging pollutants with Prunus armeniaca functionalized biochar from aqueous wastes: Experimental optimization and modeling. *Science of the Total Environment, 613–614*, 736–750.

Solanki, A., & Boyer, T. H. (2019). Physical-chemical interactions between pharmaceuticals and biochar in synthetic and real urine. *Chemosphere, 218*, 818–826.

Song, J. Y., Bhadra, B. N., & Jhung, S. H. (2017). Contribution of H-bond in adsorptive removal of pharmaceutical and personal care products from water using oxidized activated carbon. *Microporous and Mesoporous Materials, 243*, 221–228.

Tang, J., Li, H., Gong, Y., & Huang, Y. (2015). Preparation and characterization of a novel graphene/biochar composite for aqueous phenanthrene and mercury removal. *Bioresource Technology, 196*, 355–363.

Umbreen, N., Sohni, S., Ahmad, I., Khattak, N. U., & Gul, K. (2018). Self-assembled three-dimensional reduced graphene oxide-based hydrogel for highly efficient and facile removal of pharmaceutical compounds from aqueous solution. *Journal of Colloids and Interface Science, 527*, 356–367.

Uslu, M. O., Rahman, M. F., Jasim, S. Y., Yanful, E. K., & Biswas, N. (2012). Evaluation of the reactivity of organic Pollutantsduring O3/H2O2Process. *Water, Air, and Soil Pollution, 223*, 3173–3180.

Yu, Z., Peldszus, S., & Huck, P. M. (2008). Adsorption characteristics of selected pharmaceuticals and an endocrine disrupting compound-naproxen, carbamazepine and nonylphenol-on activated carbon. *Water Research, 42*, 2873–2882.

Zhang, S., Fu, R., Wu, D., Xu, W., Ye, Q., & Chen, Z. (2004). Preparation and characterization of antibacterial silver-dispersed activated carbon aerogels. *Carbon, 42*, 3209–3216.

Zhao, G., Li, J., & Wang, X. (2011). Kinetic and thermodynamic study of 1-naphthol adsorption from aqueous solution to sulfonated graphene nanosheets. *Chemical Engineering Journal, 173*, 185–190.

Web References

https://chem.libretexts.org/Reference/Reference_Tables/Spectroscopic_Parameters/Infrared_Spectroscopy_Absorption_Table

Infrared spectroscopy adsorption table, chemistry, LibreTexts